References and Notes

1. A. Ashkin, J. M. Dziedzic, J. E. Bjorkholm, S. Chu, *Opt. Lett.* **11**, 288 (1986).
2. A. Ashkin, J. M. Dziedzic, T. Yamane, *Nature* **330**, 769 (1987).
3. H. Liang, W. H. Wright, S. Cheng, W. He, M. W. Berns, *Exp. Cell Res.* **204**, 110 (1993).
4. P. Ormos, P. Galajda, *Appl. Phys. Lett.* **78**, 249 (2001).
5. H. He, M. E. J. Friese, N. R. Heckenberg, H. Rubinsztein-Dunlop, *Phys. Rev. Lett.* **75**, 826 (1995).
6. M. E. J. Friese, J. Enger, H. Rubinsztein-Dunlop, N. R. Heckenberg, *Phys. Rev. A* **54**, 1593 (1996).
7. N. B. Simpson, K. Dholakia, L. Allen, M. J. Padgett, *Opt. Lett.* **22**, 52 (1997).
8. L. Allen, M. W. Beijersbergen, R. J. C. Spreeuw, J. P Woerdman, *Phys. Rev. A* **45**, 8185 (1992).
9. M. E. J. Friese, T. A. Nieminen, N. R. Heckenberg, H. Rubinsztein-Dunlop, *Nature* **394**, 348 (1998).
10. M. E. J. Friese, H. Rubinsztein-Dunlop, J. Gold, P. Hagberg, D. Hanstorp, *Appl. Phys. Lett.* **78**, 547 (2001).
11. R. A. Beth, *Phys. Rev.* **50**, 115 (1936).
12. M. Padgett, J. Arlt, N. Simpson, L. Allen, *Am. J. Phys.* **64**, 77 (1996).
13. The experimental setup consisted of a Nd:YVO_4 laser of 300-mW power at 1064 nm. This beam is then directed through an in-house manufactured holographic element (*15*) that yielded an LG beam in its first order with an efficiency of 30%. This LG beam is then interfered with the zeroth order beam from the hologram to generate our spiral interference pattern. This pattern propagates through our optical system and is directed through either a ×40 or a ×100 microscope objective in a standard optical tweezers geometry. Typically around 1 to 13 mW of laser light was incident on the trapped structure in our optical tweezers, with losses due to optical components and the holographic element. A charge-coupled device (CCD) camera was placed above the dielectric mirror for observation purposes (Fig. 2) when the ×100 objective was used. A similar setup was used when tweezing with a ×40 objective but with the CCD camera placed below the sample slide viewing through a ×100 objective. It is important to ensure exact overlap of the light beams to guarantee that spiral arms are observed in the interference pattern—at larger angles, linear fringe patterns (with some asymmetry) can result (*15*). To set trapped structures into rotation, the relative path length between the two arms of the interferometer must be altered. We achieved this by placing a glass plate on a tilt stage in one arm. Simply by tilting this plate, we can rotate accordingly the pattern in the tweezers.
14. The tilting of the glass plate to rotate the interference pattern has a limitation when the plate reaches its maximum angle. One can, however, envisage more advanced implementations for continuous rotation using, for example, a liquid crystal phase modulator in the arm of the interferometer containing the plane wave.
15. M. A. Clifford, J. Arlt, J. Courtial, K. Dholakia, *Opt. Commun.* **156**, 300 (1998).

16. We thank the UK Engineering and Physical Sciences Research Council for supporting our work.

26 December 2000; accepted 19 March 2001

Phonon Density of States of Iron up to 153 Gigapascals

H. K. Mao,[1] J. Xu,[1] V. V. Struzhkin,[1] J. Shu,[1] R. J. Hemley,[1] W. Sturhahn,[2] M. Y. Hu,[2] E. E. Alp,[2] L. Vocadlo,[3] D. Alfè,[3] G. D. Price,[3] M. J. Gillan,[3] M. Schwoerer-Böhning,[4] D. Häusermann,[4] P. Eng,[5] G. Shen,[5] H. Giefers,[6] R. Lübbers,[6] G. Wortmann[6]

We report phonon densities of states (DOS) of iron measured by nuclear resonant inelastic x-ray scattering to 153 gigapascals and calculated from ab initio theory. Qualitatively, they are in agreement, but the theory predicts density at higher energies. From the DOS, we derive elastic and thermodynamic parameters of iron, including shear modulus, compressional and shear velocities, heat capacity, entropy, kinetic energy, zero-point energy, and Debye temperature. In comparison to the compressional and shear velocities from the preliminary reference Earth model (PREM) seismic model, our results suggest that Earth's inner core has a mean atomic number equal to or higher than pure iron, which is consistent with an iron-nickel alloy.

The phonon DOS of hexagonal close-packed (hcp) Fe at ultrahigh pressure provides information on the vibrational, elastic, and thermodynamic properties of Fe that are crucial for interpreting seismologic (*1*, *2*) and geomagnetic (*3*–*5*) observations deep in the core (*6*, *7*). The full phonon spectrum of Fe has been calculated (*8*) but needs experimental input for test and improvement. Previous phonon measurements have often been limited to partial phonon information, such as ultrasonic phonon velocities (*9*), shock-wave velocities (*10*–*12*), stress-strain relations (*9*, *13*), and zone-center E_{2g} Raman phonon spectra (*14*). Nuclear resonant inelastic x-ray scattering (NRIXS), a relatively new technique (*15*, *16*), has been applied to determine the phonon DOS of body-centered cubic (bcc) Fe at ambient pressure (*17*) and hcp Fe to 42 GPa (*18*), but these pressures are still far below the pressure found in the liquid outer core (135 to 330 GPa) and solid inner core (330 to 363 GPa). Moreover, the hcp Fe study also does not yield the correct phonon DOS; i.e., the reported Debye average phonon velocity (V_D) (*18*) is as much as 20% higher than the ultrasonic and x-ray diffraction results (*9*). Here we report a new experimental and theoretical comparison. With high-resolution NRIXS measurements, we obtained the phonon DOS of Fe at pressures beyond the core-mantle boundary of Earth. Using ab initio theory, we calculated the phonon DOS and derived elastic and thermodynamic parameters for equivalent pressures. Comparison between experiment and theory provides guidance to the development of theory for application at the pressure-temperature (*P*-*T*) range unattainable by experiments.

In order to achieve core pressures for NRIXS studies and to optimize the detection of the Fe fluorescence (*16*, *18*), we modified

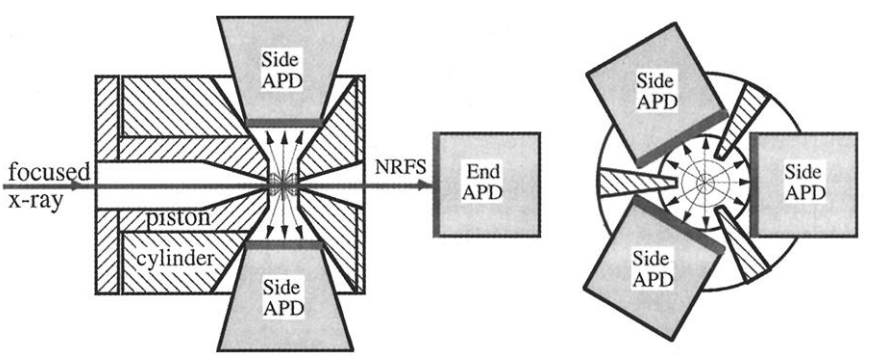

Fig. 1. Wide-angle diamond cell optimized for NRIXS at ultrahigh pressures (left, side view; right, end view). Long piston-cylinder configuration assures the alignment stability critical for reaching ultrahigh pressures. Three windows, each with a 105° equatorial and 68° azimuthal opening [resembling cells developed for neutron diffraction (*36*)], allow the collection of Fe fluorescence through the high-strength Be gaskets (*19*) over a huge (40% of the $4\pi r^2$) spherical area by tailor-fitting three APD on the side. The fourth APD at the end records the coherent nuclear forward scattering and monitors the instrument resolution function.

[1]Geophysical Laboratory and Center for High Pressure Research, Carnegie Institution of Washington, Washington, DC 20015, USA. [2]Advanced Photon Source, Argonne, IL 60439, USA. [3]University College London, Gower Street, London WC1E 6BT, UK. [4]High Pressure Collaborative Access Team (HPCAT), Advanced Photon Source, Argonne, IL 60439, USA. [5]Consortium for Advanced Radiation Sources, University of Chicago, Chicago, IL 60637. [6]Fachbereich Physik, University of Paderborn, D33095 Paderborn, Germany.

the megabar diamond cell (Fig. 1). Isotopically enriched ^{57}Fe samples were loaded in a Be gasket (*19*). No pressure medium was used. NRIXS was performed at the undulator beamline (3ID) of the Advanced Photon Source (APS) with a high-resolution (2 meV) monochromator scanning the range of ±100 meV in steps of 0.4 meV (*20*). Pressures were calibrated by the ruby scale (*21*) and confirmed by the equation of state of Fe (*13*) from x-ray diffraction, which also revealed the crystal structure and preferred orientation of the Fe samples. Data were collected at 0, 3, 25, 36, 50, 70, 112, 133, and 153 GPa in two experiments (Fig. 2). Our DOS of hcp Fe shows sharp multiple-resolved phonon peaks, sharp high-energy cut off, and velocities that match ultrasonic and x-ray diffraction values (*9*). As observed in a textural study (*22*), hcp Fe developed preferred orientation with the c axis, partially aligning to the compressional direction. However, within the statistical accuracy, no significant dependence of the phonon DOS on the preferred orientation was observed. This is consistent with the Raman phonon study of hcp Fe to 152 GPa (*9*), which indicates nearly isotropic shear phonon velocity.

Ab initio electronic structure calculations were performed on the Cray T3E at Manchester, England, to determine the phonon DOS of hcp Fe at the same pressures (*23*). Density functional theory (DFT) within the generalized gradient approximation (GGA) was used with the Projector Augmented Wave (PAW) method (*24*), as implemented in the VASP code [Vienna ab initio simulation package (*25*)] to describe the electron-core interactions, and the small displacement method was used to obtain the vibrational properties. We used supercells containing 36 atoms with an electronic k-point sampling grid of 19 to 39 k-points in the irreducible Brillouin zone. The calculated phonon DOS spectra for bcc Fe below 3 GPa compare well (within ±2 meV) with the NRIXS results (Fig. 2). For hcp Fe, the multiple peaks of the calculated and measured DOS agree qualitatively within the 2-meV resolution limits, but the theoretical DOS calculated for the nonmagnetic Fe is shifted 3 to 5 meV to higher energies, most pronounced for the low-energy branches (transversal modes and the optic E_{2g} mode). A similar discrepancy exists for the recently measured optic E_{2g} mode (*14*), pointing to an incomplete description of hcp Fe by theory, at least in the low-pressure region. At higher pressures, the difference between theoretical and measured DOS spectra reduces, especially at the high-energy cutoff energy. The noise and oscillations visible in the experimental spectra beyond the cutoff energy are a result of the normalization and multi-phonon subtraction procedures of the measured spectra by Fourier analysis, which enhances the noise of the low-count rate measurements of the microscopic samples at ultrahigh pressures.

High-pressure density (ρ), compressional

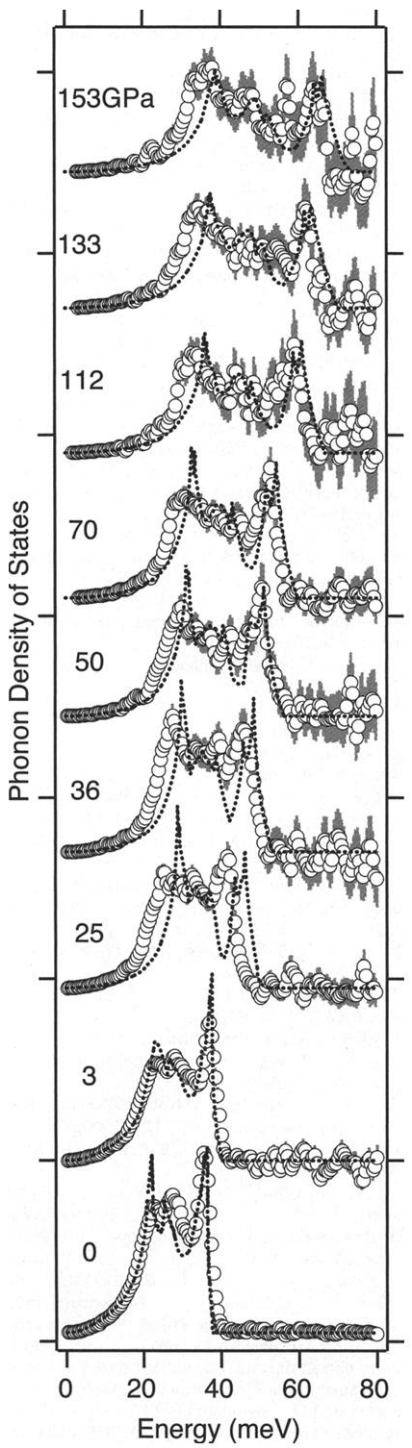

Fig. 2. Phonon DOS of Fe. Thin dotted curves, ab initio theory; circles with error bars, NRIXS data.

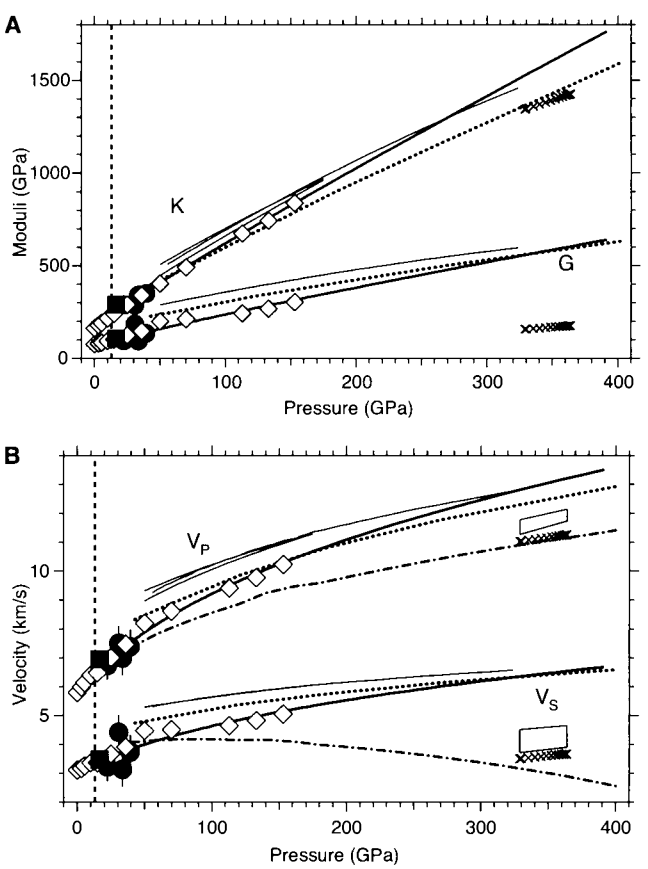

Fig. 3. (**A**) Bulk and shear moduli and (**B**) aggregate compressional and shear velocities of Fe at high pressures. Solid squares (*9*), ultrasonic data; circles, solid RXD data with Au stress calibration; open diamonds, the present NRIXS results; bold solid curves, linear-fitting of velocity as a function of density through the ultrasonic and the NRIXS data [except for *K*, which is the input values from (*13*)]; dotted curves, calculated from the slope at the gamma point of the present ab initio theoretical phonon dispersion curves; thin solid curves, first-principles calculations of Steinle-Neumann *et al.* (*29*) for nonmagnetic (nm) (upper thin curve) and antiferromagnetic (afm) (lower thin curve) phases. The afm calculations were only performed for *K*; afm curves for V_S and V_P were calculated (courtesy of Steinle-Neumann) from *K* (afm) and *G* (nm). The V_S of afm and nm are indistinguishable in this plot. The dash-dot curves are shock-wave data (*12*) at high Hugoniot temperature; crosses, inner core values form PREM (*35*); open box, linear temperature correction between Hugoniot and our curve for Fe at a range of estimated inner core geotherms [4670 to 6600 K] (*34*). The vertical line separating bcc and hcp Fe at 13 GPa is also shown in Fig. 4.

velocity (V_P), shear velocity (V_S), bulk modulus (K), and shear modulus (G) are the primary parameters observable by seismology. They are related by

$$\frac{K}{\rho} = V_P^2 - \frac{4}{3}V_S^2 \quad (1)$$

$$\frac{G}{\rho} = V_S^2 \quad (2)$$

The K and ρ have been determined by x-ray diffraction under hydrostatic conditions to 78 GPa (*26*) and nonhydrostatic conditions to 300 GPa (*13*). Parabolic fitting of the low-energy slope of the present phonon DOS provides a measure of V_D as (*27*)

$$\frac{3}{V_D^3} = \frac{1}{V_P^3} + \frac{2}{V_S^3} \quad (3)$$

thus providing the additional independent equation for defining all five parameters. As a result of the complication of multiple maxima and van Hove singularities at higher energy, the Debye parabola is best constrained at the low-energy limit, and a resolution of 2 meV is essential for approaching that limit. Equations 1 through 3 are solved for V_P, V_S, and G up to 153 GPa. Our experimental values of hcp Fe are in excellent agreement with the anchor points at 16.5 GPa and the RXD data at 20 to 39 GPa, and confirm the validity of constant K/G extrapolation (*9*) above 39 GPa.

For bcc Fe, V_P, V_S, and G determined by NRIXS and calculated from ab initio theory agree well with each other and with the ultrasonic anchor points at zero pressure (*28*). For hcp Fe, the V_P, V_S, and G calculated from the ab initio DOS (dotted curves in Fig. 2) are significantly higher than the experimental values, reflecting the higher observed energy at the initial slopes of the ab initio DOS. A similar discrepancy in the theoretical and experimental comparison of K has been noticed and successfully reduced by including the magnetic spin in calculations of an assumed antiferromagnetic (afm) phase (*29*, *30*). The afm calculation, however, is insufficient to remove the discrepancies in G, V_P, and V_S (Fig. 3). Additional theoretical considerations must be sought in order to meet additional constraints set by our experimental results of G, V_P, and V_S.

Vibrational kinetic energy (E_k), zero point energy (E_Z), vibrational heat capacity (C_{vib}), vibrational entropy (S_{vib}), and Debye temperature (Θ_D) are calculated from integration of the phonon DOS (Fig. 4). For bcc Fe, the experimental results agree well with those derived from the theoretical calculations. For hcp Fe, we again observe systematic deviations of the ab initio values at the high-energy cut off of the DOS to higher energies that correspond to higher E_k and E_Z and lower C_{vib} and S_{vib}. However, the pressure slopes of these thermodynamic parameters agree quite well.

Key parameters that control the physical states of iron-rich planetary cores (*6*) have been estimated by shock-wave measurements (*10*) and theoretical calculations (*31*–*33*) at high pressure and temperature. Those results provide information that includes both electronic and vibrational contributions. In contrast, our 300 K isothermal data constrain the end-member vibrational contribution, and the comparison with shock-wave data yields quantitative evaluation of the electronic contribution and temperature derivatives. For instance, thermoelastic parameters are obtained by comparison of our V_P and V_S with shock-wave Hugoniot (*12*). From our curves at 300 K and shock-wave curves at 8000 to 9000 K (Fig. 3), the calculated V_P and V_S of pure iron under the P-T conditions of the solid inner core (*34*) are slightly higher than the seismic PREM model (*35*). The difference is marginally within mutual uncertainties. Additional light-element alloys in the inner core would further increase this difference, whereas the addition of a heavy-element alloy, such as 5 to 10% nickel as suggested by geochemical evidence, would bring perfect agreement.

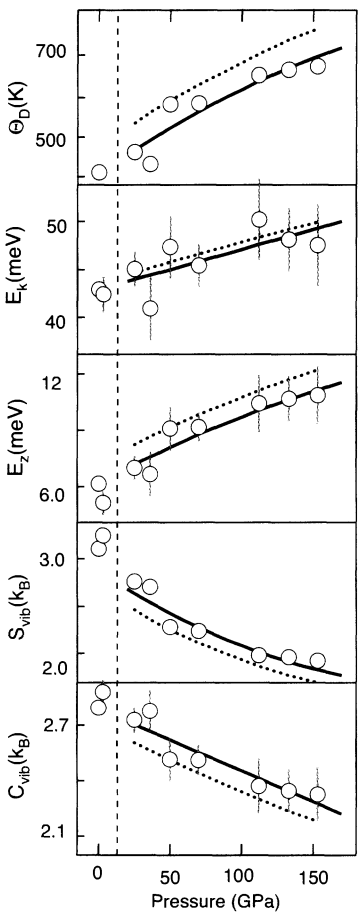

Fig. 4. Thermodynamic parameters of Fe. k_B, Boltzmann constant. Circles and solid curves, NRIXS data and fitted curves, respectively; dotted curves, ab initio calculations.

Reference and Notes

1. X. Song, D. V. Helmberger, *Science* **282**, 924 (1998).
2. W.-J. Su, A. M. Dziewonski, R. Jeanloz, *Science* **274**, 1883 (1996).
3. W. Kuang, J. Bloxham, *Nature* **389**, 371 (1997).
4. G. A. Glatzmaier, P. H. Roberts, *Science* **274**, 1887 (1996).
5. R. Ladbury, *Phys. Today* **49**, 17 (1996).
6. O. L. Anderson, *Rev. Geophys.* **33**, 429 (1995).
7. A. Jephcoat, P. Olson, *Nature* **325**, 332 (1987).
8. G. A. deWijs *et al.*, *Nature* **392**, 805 (1998).
9. H. K. Mao *et al.*, *Nature* **396**, 741 (1998).
10. G. Chen, T. J. Ahrens, *Geophys. Res. Lett.* **22**, 21 (1995).
11. C. S. Yoo, N. C. Holmes, M. Ross, *Phys. Rev. Lett.* **70**, 3931 (1993).
12. J. M. Brown, R. G. McQueen, *J. Geophys. Res.* **91**, 7485 (1986).
13. H. K. Mao, Y. Wu, L. C. Chen, J. F. Shu, A. P. Jephcoat, *J. Geophys. Res.* **95**, 21 (1990).
14. S. Merkel, A. F. Goncharov, H. K. Mao, P. Gillet, R. J. Hemley, *Science* **288**, 1626 (2000).
15. M. Seto, Y. Yoda, S. Kikuta, X. W. Zhang, M. Ando, *Phys. Rev. Lett.* **74**, 3828 (1995).
16. W. Sturhahn *et al.*, *Phys. Rev. Lett.* **74**, 3832 (1995).
17. M. Y. Hu *et al.*, *Nucl. Instrum. Meth. Phys. Res. A* **428**, 551 (1999).
18. R. Lübbers, H. F. Grünsteudel, A. I. Chumakov, G. Wortmann, *Science* **287**, 1250 (2000); R. Lübbers *et al.*, unpublished data. The NRIXS DOS of hcp Fe have been re-measured up to 40 GPa with improved spectral resolution at European Synchrotron Radiation Facility; the new data agree now with our results.
19. R. J. Hemley *et al.*, *Science* **276**, 1242 (1997).
20. X-ray beam was focused by two Pt-coated Kirkpatrick-Baez mirrors to a 5 μm by 5 μm area impinging on the ^{57}Fe sample at high pressures. The elastic and inelastic resonant excitations were observed by collecting the delayed Fe K_α and K_β fluorescences with three side avalanche photodiode detectors (APD) (Fig. 1) Typically, 20 to 30 NRIXS spectra were collected for 1 hour each, summed, and converted to phonon DOS spectra (*17*).
21. H. K. Mao, P. M. Bell, J. Shaner, D. Steinberg, *J. Appl. Phys.* **49**, 3276 (1978).
22. H.-R. Wenk, S. Matthies, R. J. Hemley, H. K. Mao, J. Shu, *Nature* **405**, 1044 (2000).
23. L. Vocadlo, J. Brodholt, D. Alfé, G. D. Price, *Geophys. Res. Lett.* **26**, 1231 (1999).
24. P. E. Blöchl, *Phys. Rev. B* **50**, 17 (1994).
25. G. Kresse, J. Furthmüller, *Phys. Rev. B* **54**, 11 (1996).
26. A. P. Jephcoat, H. K. Mao and P. M. Bell, *J. Geophys. Res.* **91**, 4677 (1986).
27. G. Simmons, H. Wang, *Single Crystal Elastic Constants and Calculated Aggregate Properties* (MIT Press, Cambridge, MA, 1971).
28. M. W. Guinan, D. N. Beshers, *J. Phys. Chem. Solids* **29**, 541 (1968).
29. G. Steinle-Neumann, L. Stixrude, R. E. Cohen, *Phys. Rev. B* **60**, 791 (1999).
30. L. Stixrude, R. E. Cohen, *Science* **267**, 1972 (1995).
31. L. Stixrude, E. Wasserman, R. E. Cohen, *J. Geophys. Res.* **102**, 24 (1997).
32. L. Vocadlo, J. Brodholt, D. Alfé, M. J. Gillan, G. D. Price, *Phys. Earth Planet. Inter.* **117**, 123 (2000).
33. E. Wasserman, L. Stixrude, R. E. Cohen, *Phys. Rev. B* **53**, 8296 (1996).
34. J.-P. Poirier, *Introduction to the Physics of the Earth Interior* (Cambridge Univ. Press, Cambridge, 2000).
35. A. Dziewonski, D. L. Anderson, *Phys. Earth Planet. Inter.* **25**, 297 (1981).
36. V. P. Glazkov *et al.*, *JETP Lett.* **47**, 661 (1988).

37. We thank R. E. Cohen, G. Steinle-Neumann, and L. Stixrude for their theoretical results and constructive discussion; Yu. Shvydko for APD detectors; J. Hu for x-ray diffraction; and APS and National Synchrotron Light Source (NSLS) for synchrotron beam time. Supported by NSF under grants EAR9706624 and Center for High Pressure Research, by DOE-BES under contract W-31-109-ENG-38, and by BMBF under project 05SK8PPA.

22 November 2000; accepted 21 March 2001